

## Investigating the relationship between internal short circuit and thermal runaway of lithium-ion batteries under thermal abuse condition

Dongsheng Ren<sup>a,b</sup>, Xuning Feng<sup>b</sup>, Lishuo Liu<sup>b</sup>, Hungjen Hsu<sup>b</sup>, Languang Lu<sup>b</sup>, Li Wang<sup>a,b</sup>, Xiangming He<sup>a,b,\*</sup>, Minggao Ouyang<sup>b,\*</sup>

<sup>a</sup> Institute of Nuclear and New Energy Technology, Tsinghua University, Beijing 100084, China

<sup>b</sup> State Key Laboratory of Automotive Safety and Energy, Tsinghua University, Beijing 100084, China



### ARTICLE INFO

**Keywords:**  
Energy storage  
Lithium-ion battery  
Battery safety  
Thermal runaway  
Internal short circuit

### ABSTRACT

Thermal runaway, a critical problem that hinders the application of lithium-ion battery, is always a thermal-electrical coupled process where exothermic chemical reactions and internal short circuit coincide and interact with each other. Clarifying the contributions of chemical reactions and internal short circuit to thermal runaway is crucial for developing safer lithium-ion battery. In this paper, the relationship between internal short circuit and thermal runaway of lithium-ion battery under thermal abuse condition is investigated through experimental and modeling approaches. Internal short circuit is observed to happen before thermal runaway but leads to little heat generation during thermal abuse test of a lithium-ion battery with  $\text{Li}(\text{NiCoMn})_{1/3}\text{O}_2$  cathode. Liquid-nitrogen-ceased thermal runaway test and postmortem analysis are designed to characterize the cause of internal short circuit. Thermal shrinkage of the separator is found responsible for the occurrence of internal short circuit. However, the joule heat from internal short circuit is limited by the sharp-increased battery resistance and thus contributes little to battery thermal runaway. Moreover, exothermic reactions between the anode and electrolyte are determined as the trigger of thermal runaway of the  $\text{Li}(\text{NiCoMn})_{1/3}\text{O}_2$ -based battery, in contrast to the conventional views that the highly reactive oxygen released from cathode or internal short circuit is the critical factor for thermal runaway of lithium-ion battery. Finally, a model-based discussion on the effect of internal short circuit on the thermal runaway of batteries with different designs is presented. The results provide new insights into battery thermal runaway mechanism and can benefit the safety design of lithium-ion battery.

### 1. Introduction

Transportation electrification has been considered an effective solution to save modern society from energy crisis and environmental pollution [1,2]. The energy storage systems of vehicles (including cars, trains, ships, and aircraft) have been changing from fossil fuels to electrochemical energy storage systems [3–6]. Lithium-ion battery is the most widely-used electrochemical energy storage system in electric vehicles, considering its high energy/power density and long cycle life [7–9]. However, with the large-scale application of electric vehicles, safety accidents associated with thermal runaway (TR) of lithium-ion battery happened occasionally, hindering consumer's confidence in electric vehicles [10–12]. Efforts are urgently required to investigate the TR of lithium-ion battery to develop safer electric vehicles.

TR of lithium-ion battery can be induced under several abuse conditions, including mechanical abuse [13–15], electric abuse [16,17], and thermal abuse [18,19]. Mechanical abuse can trigger internal short circuit (ISC), leading to electric abuse, whereas electric abuse results

in joule heat generation and initiate thermal abuse [20]. Series of exothermic reactions occur one after another inside the battery under thermal abuse condition. The reactions further generate a considerable amount of heat, forming the self-accelerated “Heat-Temperature-Reaction(HTR)” loop and resulting in battery TR finally [6,21]. The HTR loop is the root cause of battery thermal runaway and should be fully understood to improve the safety performance of lithium-ion battery.

Researchers have investigated the TR mechanism of lithium-ion battery through tests on both cells and components (i.e., cathode, anode, and electrolyte). Doughty et al. [22,23] has pioneered the use of accelerating rate calorimetry (ARC) to investigate the TR behaviors of 18,650 lithium-ion batteries and summarized possible exothermic reactions inside the battery at different stages of TR process. Feng et al. [24–26] has summarized three characteristic temperatures  $\{T_1, T_2, T_3\}$  as comparable indexes to evaluate the thermal safety of lithium-ion batteries with different chemistries, and interpreted the mechanisms that were responsible for the characteristic temperature phenomena. The

\* Corresponding authors.

E-mail addresses: [rends@tsinghua.edu.cn](mailto:rends@tsinghua.edu.cn) (D. Ren), [hexm@tsinghua.edu.cn](mailto:hexm@tsinghua.edu.cn) (X. He), [ouymg@tsinghua.edu.cn](mailto:ouymg@tsinghua.edu.cn) (M. Ouyang).

onset temperature of self-heating, i.e.  $T_1$ , is usually associated with the decomposition of solid electrolyte interphase (SEI) film on anode at around 70–100°C [27]. The reaction between lithiated graphite and electrolyte begins once the SEI film cannot protect the anode from direct exposure to the electrolyte, leading to further temperature rise in lithium-ion battery [28,29]. The cathode materials start to decompose and release oxygen when battery temperature increases to around 200°C [30–32]. The highly reactive oxygen will react with organic solvents and lithiated graphite, generating a large amount of heat [33–35]. ISC will also happen and release joule heat once the separator fails to prevent direct contact of cathode and anode [36,37]. Those exothermic reactions form the HTR loop and finally lead to TR of lithium-ion battery.  $T_2$  indicates the onset of TR and is usually defined as the temperature at which the battery temperature rate exceeds  $1^{\circ}\text{C}\cdot\text{s}^{-1}$ . The triggering mechanism of  $T_2$  is complicated and is usually related to several exothermic processes, including 1) joule heat generation from ISC [17,24]; 2) the reactions between electrolyte/anode and oxygen released from cathode materials [34,35,38]; 3) the reaction between plated lithium and electrolyte [39–41].  $T_3$  is the maximum temperature and corresponds to the total energy release during TR process. Clarifying the contribution of each exothermic process can help to regulate the heat generation during battery TR process and improve battery safety efficiently.

However, the contributions of ISC and exothermic reactions to TR of lithium-ion battery are challenging to separate, as ISC and exothermic reactions always proceed concurrently. ISC is regarded as the common feature of TR under different abuse conditions [6,42,43]. Under mechanical abuse condition (such as nail penetration and crush), ISC is usually induced by deformation of separator, and releases a large amount of joule heat that can trigger TR directly [13,44,45]. Li/Cu dendrite that forms under overcharge/over-discharge condition can piece separator and leads to ISC [46,47], and the joule heat generation from ISC mainly depends on the ISC resistance [43,47,48]. Under thermal abuse condition, ISC is usually caused by shrinkage of separator [49]. For the battery using PE separator, ISC usually happens simultaneously with TR during thermal abuse and is considered as the root cause of TR [24,37,49]. However, with the application of more thermal stable separator (such as ceramic-coated separator and non-woven separator), ISC was found to happen before or even after TR during thermal abuse tests [34,50], making the relationship between ISC and TR unclear.

In this paper, the relationship between ISC and TR under thermal abuse condition is investigated through experimental and modeling approaches. ISC was first found to happen before TR during ARC tests on a commercial pouch lithium-ion battery, but had little influence on battery temperature rate profile. Liquid-nitrogen-ceased TR test and subsequent postmortem analysis were then carried out to characterize the cause of ISC and its contribution to total heat generation. Moreover, ARC tests on partial cells composed of various parts of battery components were conducted to find out the root cause of battery TR. Finally, a discussion on the effect of internal short circuit on thermal runaway of batteries with different designs is carried out using a 3D electrochemical-thermal coupled model.

## 2. Experiments

### 2.1. Cell information and characterization

A commercial pouch lithium-ion battery with a nominal capacity of 24Ah was investigated in this paper. The battery had  $\text{Li}(\text{NiCoMn})_{1/3}\text{O}_2$  cathode and graphite anode, and a polyethylene (PE)-based separator with ceramic coating. The electrolyte used in the 24Ah battery was composed of 1.0 M  $\text{LiPF}_6$  in ethylene carbonate (EC) / ethyl methyl carbonate (EMC) / dimethyl carbonate (DMC) (1:1:1 in volume). Prior to TR tests, the capacity of the tested battery was characterized by cycling three times between 2.5 and 4.2 V under the constant current (1/3C)-constant voltage (4.2 V, 1/20C cut-off current) charging and constant current (1/3C) discharging profile at room temperature.

### 2.2. Thermal runaway tests using extended volume accelerated rate calorimetry

TR tests were performed on the lithium-ion batteries using an extended volume accelerated rate calorimetry (EV-ARC) manufactured by Thermal Hazard Technology. Before TR test, the tested batteries were fully charged using the constant current – constant voltage charging protocol. Two cells connected in parallel were utilized for each TR test, with K-type thermocouples inserted between the two cells to monitor the internal temperature, as in our previous paper [21,51]. The battery voltage was recorded using a data logger by Hitachi.

The EV-ARC system was well-calibrated using an Al block before TR tests. TR tests were conducted in the typical heat-wait-seek mode. The start temperature and temperature step were set as 40°C and 5°C, respectively, whereas the wait time and seek time were 30 min and 20 min, respectively. Once the battery temperature rate in the seek period exceeds the preset sensitivity ( $0.01^{\circ}\text{C min}^{-1}$  in this paper), the EV-ARC system will go into the exotherm mode to track battery temperature rise and maintain the adiabatic condition until TR happens.

### 2.3. Liquid-nitrogen-ceased thermal runaway test and postmortem analysis

Liquid-nitrogen(LN)-ceased TR test was conducted to in-depth investigate the relationship between ISC and TR. An EV plus ARC was used for this test, considering its feasibility for connecting with a liquid nitrogen tank outside the chamber. The EV plus ARC system was also operated under the heat-wait-seek mode. During the LN-ceased TR test, the battery temperature and voltage were monitored simultaneously. Once the battery voltage dropped sharply to less than 1 V, liquid nitrogen was injected into the ARC chamber to freeze the battery and stop the TR process.

The cooled battery was rapidly transferred into an argon-filled glove box and dismantled to harvest the battery components for subsequent analysis. Scanning electron microscopy (SEM) - Energy dispersive spectrometer (EDS) analysis was conducted to characterize the morphology and composition of battery components (cathode, anode, and separator), using a Zeiss Merlin field emission scanning electron microscope with EDS.

Moreover, NCM/Li and Gr/Li coin cells were assembled using the harvested cathode and anode materials paired with lithium metal counter electrode to investigate the changes of electrode electrochemical properties after ISC. Coin cells with NCM as working electrode and graphite as counter electrodes were also fabricated, denoted as NCM/Gr. The coin cells were tested with a current density of  $0.088\text{mA}\cdot\text{cm}^2$  (around 1/30C) at 25 °C. The NCM/Li and NCM/Gr coin cells were first discharged to 2.8 V and 2.5 V, respectively, while those with Gr/Li electrodes were first charged to 2.0 V. The coin cells were then cycled three times to measure their capacities, with the voltage range for NCM/Li, Gr/Li, and NCM/Gr coin cells set as 2.8–4.3 V, 0.01–2.0 V, and 2.5–4.2 V, respectively. Electrochemical impedance spectroscopy (EIS) test was also conducted on the NCM/Gr coin cells to characterize the changes in battery impedance. Coin cells using electrodes from a pristine battery were also fabricated and tested for comparison.

### 2.4. Partial cells fabrication and TR tests

Cells composed of parts of battery components, denoted as partial cells, were assembled and tested to characterize the contributions of the cathode-electrolyte, anode-electrolyte, and cathode-anode thermodynamic systems during TR process [25,26,39], as in Fig. 1. The fabrication process of partial cells was carried out in the glove box with oxygen and water contents less than 0.1 ppm. As shown in Fig. 1, 15 pieces of cathode and 16 pieces of anode were harvested from a fully-charged battery and then cut into six parts. Before the fabrication of the partial cells, the cathode and anode were soaked with DMC for 2 h and dried for 12 more hours to eliminate the residual electrolyte. Three kinds of

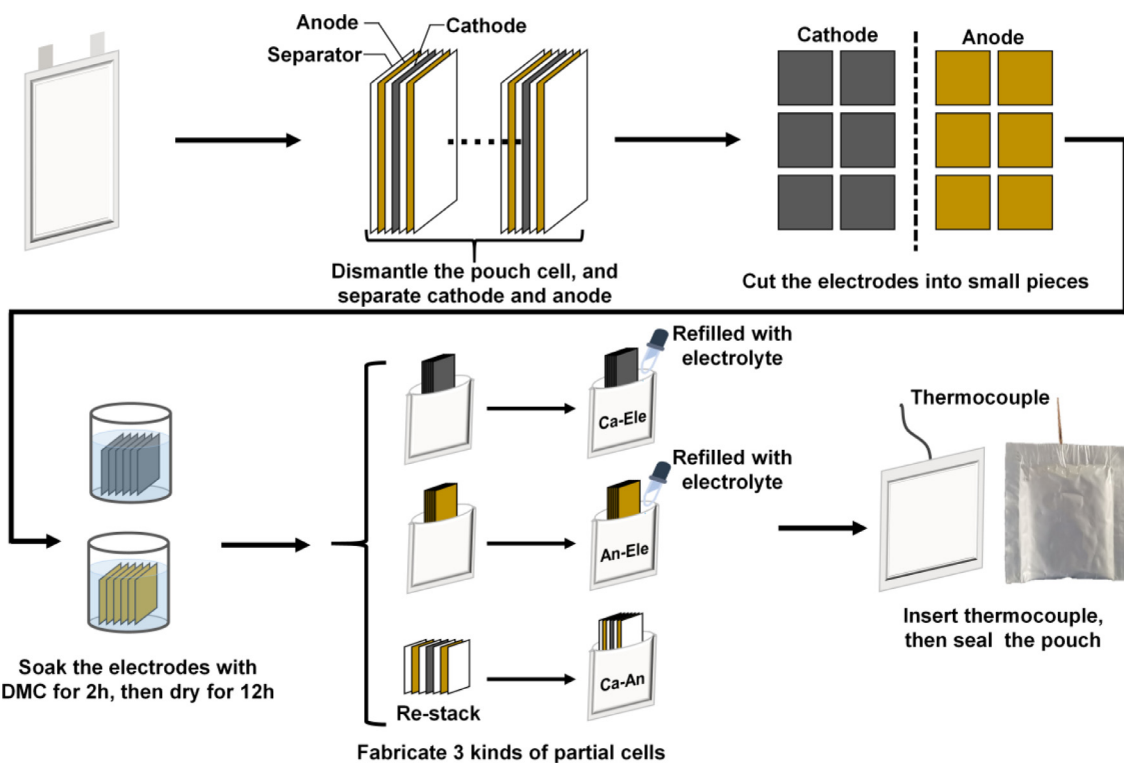


**Fig. 1.** Schematic of the fabrication process of partial cells. (Top) A fully charged lithium-ion battery was dismantled in the glove box, and the cathode and anode were separated and cut into small pieces; (Bottom) The electrodes were soaked with DMC to eliminate residual electrolyte. Then, three kinds of partial cells with different mixtures of cell components were assembled.

**Table 1**

Critical temperatures during TR tests.

Test No.	$T_1$ / °C	$T_2$ / °C	$T_3$ / °C
1	72.39	213.3	829.3
2	72.11	210.2	823.3
3	67.79	206.1	836.2

partial cells were assembled in this paper, denoted as Ca-Ele, An-Ele, and Ca-An, as shown in Fig. 1. For the Ca-Ele and An-Ele partial cells, electrolyte was refilled into the pouch bags made of aluminum-plastic film, with the same mass ratios between the cathode, anode, and electrolyte determined from battery specification. In the Ca-An partial cell, 15 cathode pieces and 16 anode pieces were re-tacked using a PE/PP/PE separator manufactured by Celgard. The partial cells were resealed in the glove box after inserting K type thermocouples. TR tests using the same procedures in Section 2.2 were performed on the three partial cells to study the thermal stability of different thermodynamic systems.

### 3. Results and discussions

#### 3.1. Battery thermal runaway behaviors

Three repetitive TR test results are presented in Fig. 2. The three temperature rate profiles overlapped with each other, indicating excellent repeatability of the TR tests. Three critical temperatures, i.e.,  $T_1$ ,  $T_2$  and  $T_3$ , are derived from the test results to evaluate the TR performance of lithium-ion battery.  $T_1$  is the onset temperature of self-heating and is defined as the temperature at which the battery self-heating rate exceeds  $0.01\text{ }^{\circ}\text{C min}^{-1}$ .  $T_2$  represents the onset temperature of TR, and is identified as the temperature at which the battery temperature rate becomes higher than  $1\text{ }^{\circ}\text{Cs}^{-1}$  [24].  $T_3$  is the maximum temperature [25]. The three TR tests showed repeatable  $T_1$ ,  $T_2$ , and  $T_3$ , as shown in Table 1.

As shown in Fig. 2(a), the battery exhibited detectable self-heating at around  $70\text{ }^{\circ}\text{C}$ , and TR occurred when the temperature reached around  $210\text{ }^{\circ}\text{C}$ , bringing the battery temperature to higher than  $800\text{ }^{\circ}\text{C}$  in a short time.

The variations of battery voltage during TR process are compared in Fig. 3. During TR process, a rapid decrease in battery voltage usually indicates massive ISC inside the battery [52]. As shown in Fig. 3, the time sequence of ISC and TR varied in the three ARC tests. ISC coincided with TR in Test No.1 (Fig. 3(a)), while ISC happened before TR in Test No. 2 and 3 with the time interval  $\Delta t_{\text{ISC}}$  larger than 300 s, as in Fig. 3(c) and (e). The same phenomenon can be found in temperature sequence, as in Fig. 3(b), (d) and (f). The ISC temperature  $T_{\text{ISC}}$  equaled  $T_2$  in Test No.1, while  $T_{\text{ISC}}$  was around  $30\text{ }^{\circ}\text{C}$  lower than  $T_2$  in Test No. 2 and 3. Moreover, in Test No. 2 and 3, the battery voltage fluctuated when the temperature exceeded  $T_{\text{ISC}}$ , indicating continuous ISC inside the battery. Though the time sequences between ISC and TR were different, the three tests exhibited the same temperature rate profiles, as in Fig. 2(b). That demonstrates that ISC led to little heat generation, contradicting with the common view that ISC will release a significant amount of joule heat and induce TR directly during thermal abuse [6,24,51,53–56]. The ISC mechanism and the relationship between ISC and TR require further clarification.

#### 3.2. Liquid-nitrogen-ceased thermal runaway test results

Liquid nitrogen cooling was utilized to freeze the battery when ISC occurred, as shown in Fig. 4(a). An internal-shorted battery was then saved from TR, and the internal changes of battery components were characterized. The LN-cooled battery swelled severely, and the pouch bag ruptured, as shown in Fig. 4(b). The mass of the battery decreased from 505 g to 453.7 g, indicating that nearly all the low-boiling-point solvents (EMC (28.8 g) and DMC (24.9 g)) have evaporated. The battery voltage dropped from 3.964 V to 0 V when ISC happened. After LN

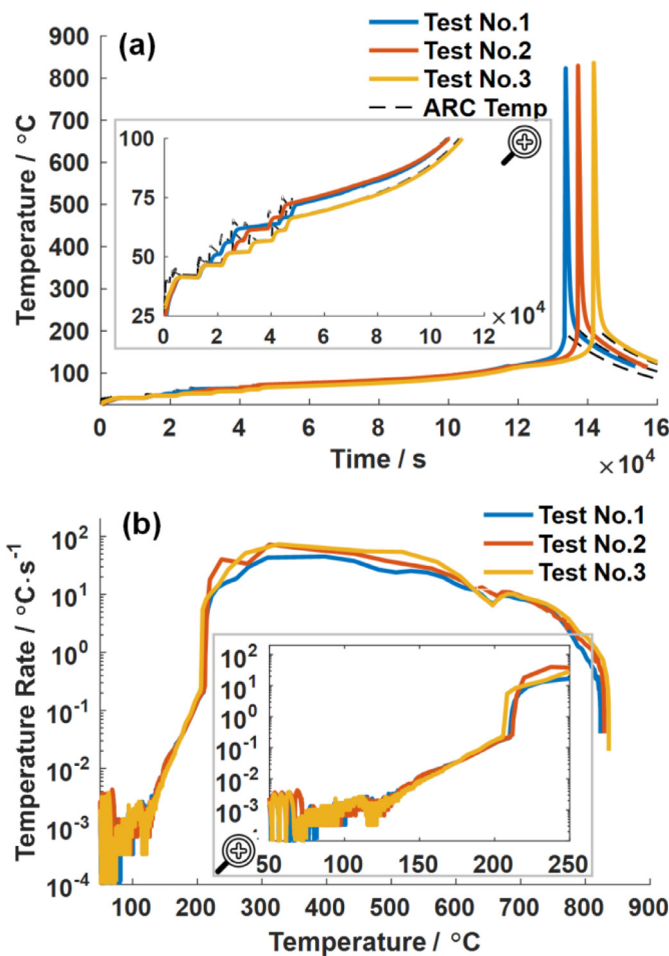


**Fig. 2.** Three repetitive TR test results. (a) temperature profiles; (b) temperature rate profiles.

cooling, the battery resistance @1 kHz increased to  $1.048\Omega$ , around 700 times larger than that of the pristine battery ( $1.5m\Omega$ ).

The LN-cooled battery was dismantled in the glove box, as shown in Fig. 4(c). The battery was dried out with little evidence of liquid electrolyte, consistent with the mass loss. The anode color changed into crimson from golden (the color of pristine fully-charged graphite [40,57]), indicating possible side reactions or self-discharging in the anode [58]. The separator adhered to the cathode and exhibited severe shrinkage. Large cracks can be found in the middle of the separator, as shown in Fig. 4(c). ISC was observed at the edge as parts of the cathode were exposed and contacted with the anode, accounting for the rapid drop of battery voltage during the TR tests. The shrinkage of the separator was mainly caused by PE melting [49,59], which happened when the battery temperature exceeded around 130°C. Though ceramic coating can help to lower the shrinkage rate, the separator still kept shrinking with the increase of temperature, leading to increased risk of ISC [49,59]. Therefore, we can conclude that ISC did happen inside the battery during TR test, resulting from thermal shrinkage of the separator. However, as shown in Figs. 2 and 3, the battery exhibited no increase in temperature rate when ISC occurred, demonstrating that little joule heat was generated from ISC.

### 3.3. postmortem analysis of the liquid-nitrogen-cooled battery

Coin cells using electrodes from the LN-cooled battery were tested to identify the changes in battery electrochemical properties, as presented in Table 2. It should be noted that the numbers presented in

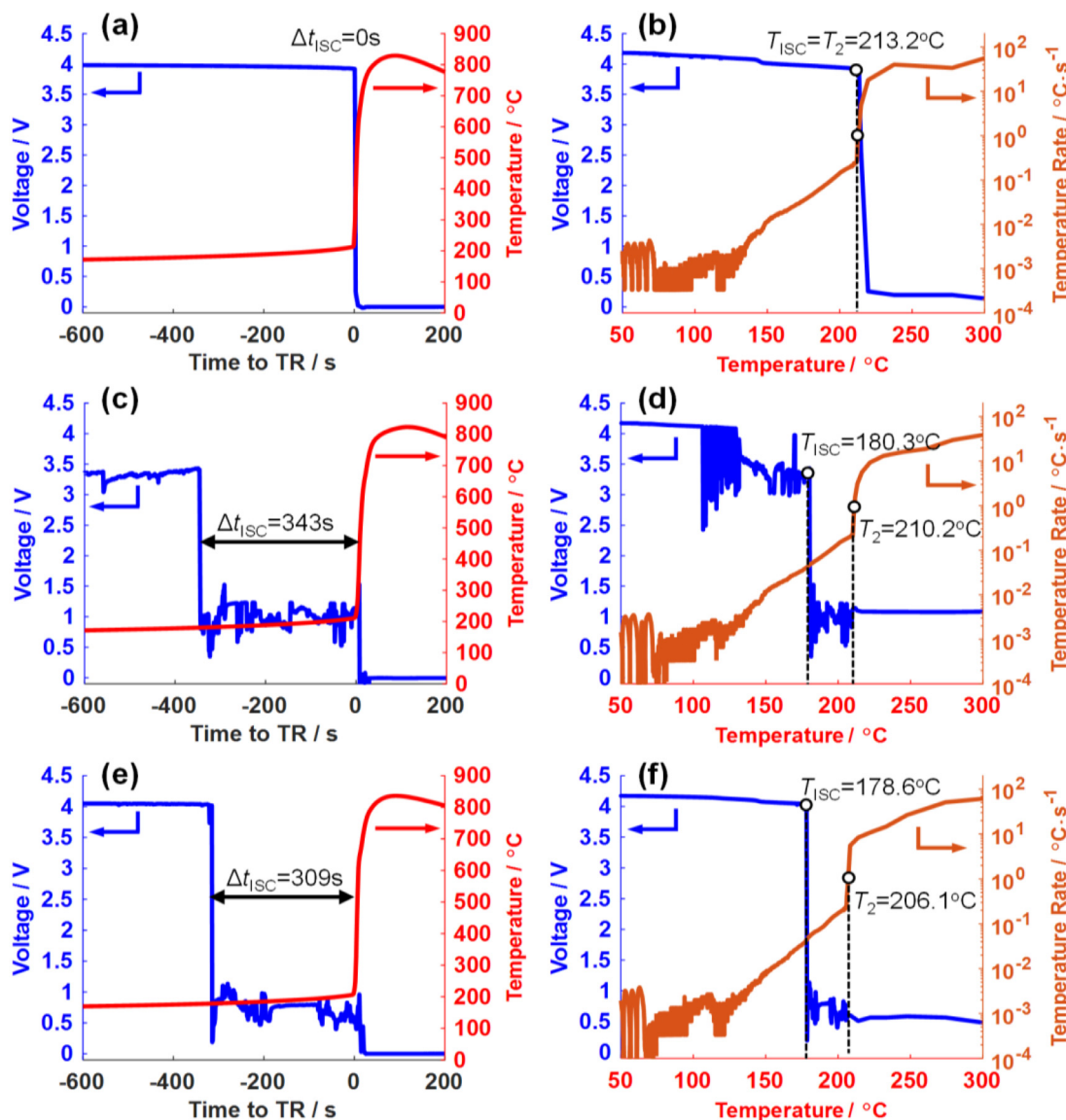
Table 2 are the average test results of three coin cells with the same materials. The LN-cooled NCM/Li coin cell showed decreased initial open circuit voltage (OCV) and initial discharge capacity, convincing that self-discharging happened on the battery. The LN-cooled NCM also suffered from capacity degradation. For the anode, the Gr/Li coin cells exhibited the most severe degradation of initial charge capacity and total capacity compared to NCM/Li and NCM/Gr coin cells, mainly due to the decomposition of SEI film and the reaction between lithiated graphite and electrolyte [58]. The NCM/Gr had an initial OCV of 3.934 V, closed to the battery voltage (3.964 V) when ISC occurred. The initial discharge capacity and total capacity of the LN-cooled NCM/Gr coin cell remained more than 90% of those of pristine NCM/Gr coin cell. That demonstrates that most of the chemical energy was stored inside the battery rather than released during ISC, consistent with the changes in temperature rate profiles.

Fig. 5 shows the EIS results of the fully-charged NCM/Gr coin cells. The LN-cooled NCM/Gr coin cells exhibited much larger impedance compared to the pristine NCM/Gr coin cells, despite the inconsistent test results due to inhomogeneous degradation. The EIS results demonstrate that the LN-cooled cathode and anode suffered from significant increases of impedance, as the same separator and electrolyte were used in different coin cells.

SEM images of the electrodes taken from pristine and LN-cooled batteries are presented in Fig. 6. Intact particles and pores with clear boundaries can be observed in the pristine cathode and anode. In contrast, the LN-cooled cathode and anode showed thick deposits on the surface and severe porosity reduction, as in Fig. 6(e) and (f). Porosity reduction will lead to a significant increase of impedance and decrease of capacity in the LN-cooled electrodes, consistent with the results presented in Table 2 and Fig. 5. The composition of the deposits on cathode and anode surface was characterized by EDS, as showed in Table 3. The LN-cooled cathode showed a ten times increase of F and P compared to the pristine cathode, indicating that the deposits on the cathode surface mainly originated from decomposition of LiPF<sub>6</sub> at elevated temperature [60]. The deposits had covered the cathode surface, resulting in a lower content of transition metal (Mn, Co, and Ni). For the anode, the content of O, F, and P also increased after LN cooling, while the content of C decreased, resulting from the side reactions between anode and electrolyte [61]. Moreover, a small amount of transition metal was detected on the surface of the LN-cooled anode, indicating transition metal dissolution and deposition during TR process [34]. According to the SEM-EDS analysis, side reactions associated with electrolyte happened on both of the LN-cooled cathode and anode, leading to degradation in cathode and anode, as well as increase of battery impedance.

SEM images of the pristine and LN-cooled separator are presented in Fig. 6(c), (d), (g), and (h). The two sides of the separator showed different morphology. One side was bare PE with an interconnected porous structure, while another side was coated with Al<sub>2</sub>O<sub>3</sub> ceramic particles. The shutdown function was triggered in the LN-cooled separator, with the pores completely closed due to PE melting, as shown in Fig. 6(g) and (h). The shutdown behavior of separator led to a sharp increase of battery impedance and can help to improve battery tolerance to abuse conditions [62].

Summarized from the EIS and SEM-EDS results, the battery suffered from significant impedance increase during TR process, resulting from the following reasons: 1) severe depletion of electrolyte due to solvents evaporation and side reactions on both cathode and anode surface; 2) formation of thick deposits and porosity reduction in both cathode and anode; 3) shutdown of separator. Variation of battery resistance (@1 kHz) during ARC Tests No.3 was measured to verify the above findings, as presented in Fig. 7. The battery resistance was  $1.5m\Omega$  at the beginning of TR process and increased to  $0.117\Omega$  at around 130°C, due to evaporation of low-boiling-point solvents (EMC and DMC) and rupture of the pouch bag. As battery temperature exceeded 140°C, the battery resistance increased rapidly and peaked at  $1.808\Omega$ , 1000 times larger than the initial value. The battery resistance



**Fig. 3.** Comparison of the thermal/electric behaviors during the three TR tests. (a), (c) and (e) Voltage/temperature vs. time profiles of Test No.1, 2 and 3; (b), (d) and (f) Voltage/temperature rate vs. temperature profiles of Test No.1, 2 and 3. In Test No.1, ISC happened simultaneously with TR in both time and temperature sequences. In Test No.2, ISC happened 343 s before TR, and  $T_{\text{ISC}} = 30^{\circ}\text{C}$  lower than  $T_2$ ; In Test No.3, ISC happened 309 s before TR, and  $T_{\text{ISC}}$  was 27.5°C lower than  $T_2$ .

**Table 2**

Tests results of coin cells using electrodes from pristine and LN-cooled battery.

	Pristine battery			LN-cooled battery		
	NCM/Li	Gr/Li	NCM/Gr	NCM/Li	Gr/Li	NCM/Gr
Initial OCV / V	4.179	0.0902	4.119	3.979	0.0934	3.934
Initial charge (discharge) capacity / mAh·cm <sup>-2</sup>	2.829	2.728	2.711	2.476	1.986	2.468
Retention rate / %	/	/	/	87.52	72.80	91.04
Total capacity / mAh·cm <sup>-2</sup>	3.205	3.289	3.119	3.019	2.995	2.870
Retention rate / %	/	/	/	94.17	91.06	91.97

kept larger than  $1.35\Omega$  until  $T_{\text{ISC}}$ , after which the battery electric circuit became unstable and was broken when TR occurred. The extremely large battery resistance limited the short circuit current  $I_{\text{ISC}}$  and the consequent joule heat  $Q_{\text{ISC}}=I_{\text{ISC}}^2 \cdot R_{\text{to}}$  to a small value during ISC, and thus no visible increase was observed in the temperature rate profile. Therefore, we can conclude that ISC is not the initiation of TR during the ARC test, and the underlying TR mechanism requires further investigation.

### 3.4. Identification of thermal runaway mechanism

TR tests on three partial cells were conducted to clarify the TR mechanism of the tested battery. The test results are compared in Fig. 8, and the critical temperatures are presented in Table 4. The An-Ele and Ca-An partial cells all went to TR with the  $T_3$  higher than  $750^{\circ}\text{C}$ , while the Ca-Ele partial cell had a  $T_3$  of  $355.3^{\circ}\text{C}$  and maximum temperature rate of  $0.186^{\circ}\text{C} \cdot \text{s}^{-1}$ , less than the criterion of TR ( $1^{\circ}\text{C} \cdot \text{s}^{-1}$ ). That indicates

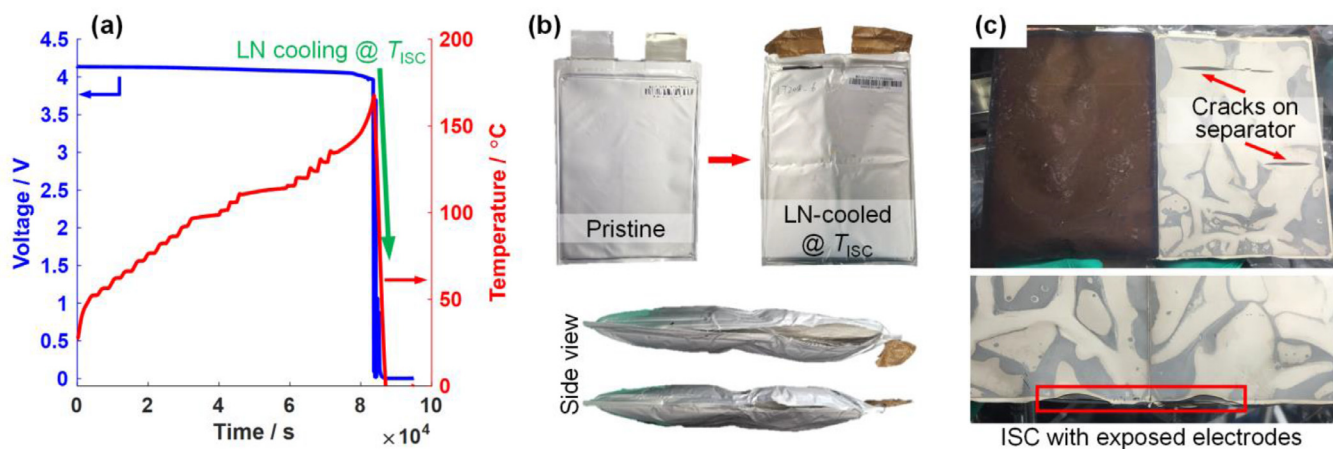


**Fig. 4.** LN-ceased TR test results. (a) variations of battery voltage and temperature during the LN-ceased TR test. The tested battery was cooled down when ISC occurred; (b) appearance of the LN-cooled battery. The battery swelled severely, and the pouch bag ruptured; (c) internal changes of the LN-cooled battery. The anode color changed into crimson, and the separator showed severe shrinkage, resulting in cracks in the middle and ISC at the edge.

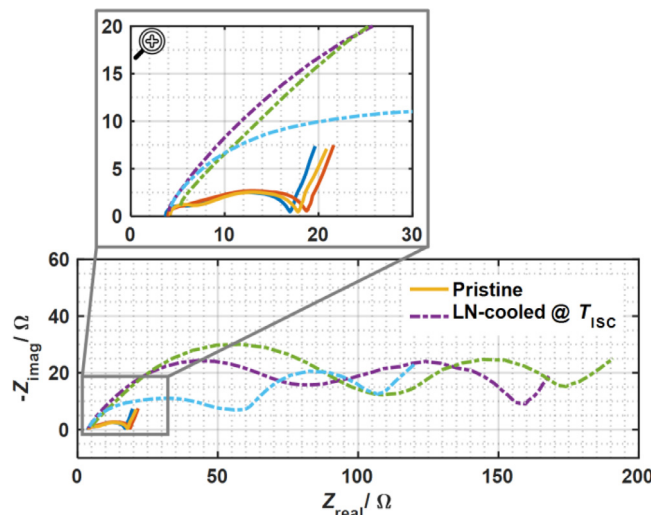


**Fig. 5.** EIS results of fully-charged NCM/Gr coin cells using electrodes from pristine and LN-cooled batteries. The LN-cooled NCM/Gr coin cells showed significant increases in impedance.

**Table 3**  
EDS analysis of the pristine and LN-cooled electrodes.

Sample	Element content / wt.%							
	C	O	F	P	Mn	Co	Ni	
Pristine	Cathode	19.69	24.12	2.74	0.15	18.08	17.89	17.34
	Anode	84.83	8.88	5.37	0.92	0	0	0
LN-cooled @ T <sub>ISC</sub>	Cathode	17.84	17.31	27.53	5.26	10.80	10.61	10.65
	Anode	63.43	16.76	16.42	2.92	0.08	0.16	0.22

**Table 4**  
Comparison of the critical temperatures of partial cells and full cell during TR process.

Sample	T <sub>1</sub> / °C	T <sub>2</sub> / °C	T <sub>3</sub> / °C
Partial Cell	Ca-Ele	101.6	N/A
	An-Ele	81.66	243.5
	Ca-An	81.45	314.7
Full Cell (Test No.1)	72.39	213.3	829.3

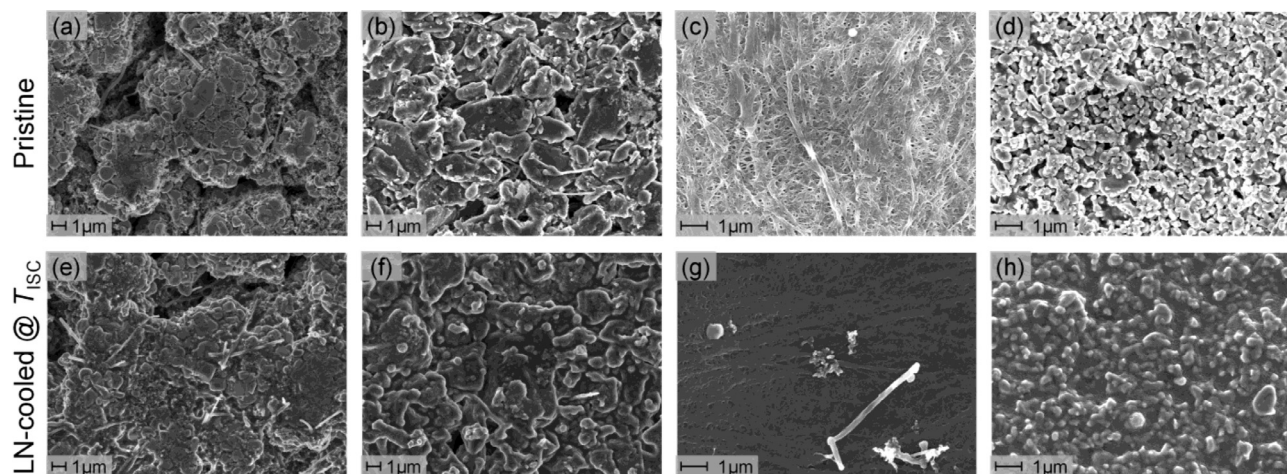


**Fig. 6.** SEM images of cathode, anode and separator from pristine and LN-cooled batteries. (a), (e) cathode. The LN-cooled cathode showed thick deposits on the surface and reduced porosity; (b), (f) anode. The LN-cooled anode also had thick deposits and reduced porosity; (c), (g) PE side of separator; (d), (h) ceramic-coated side of separator. The separator suffered from PE melting and thus pore closure.

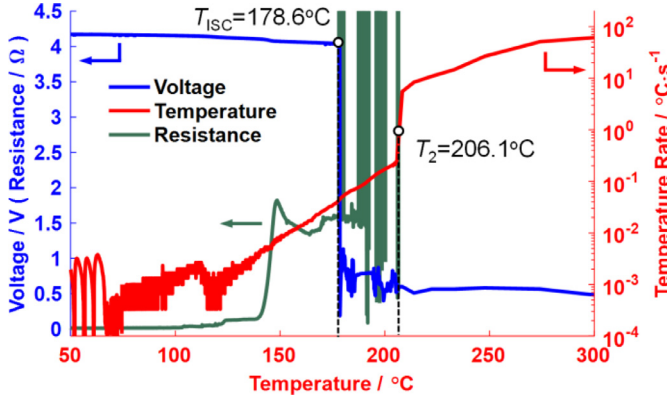


**Fig. 7.** Variations of battery resistance, voltage and temperature rate during TR test No.3. Sharp increase of battery resistance can be observed before ISC.

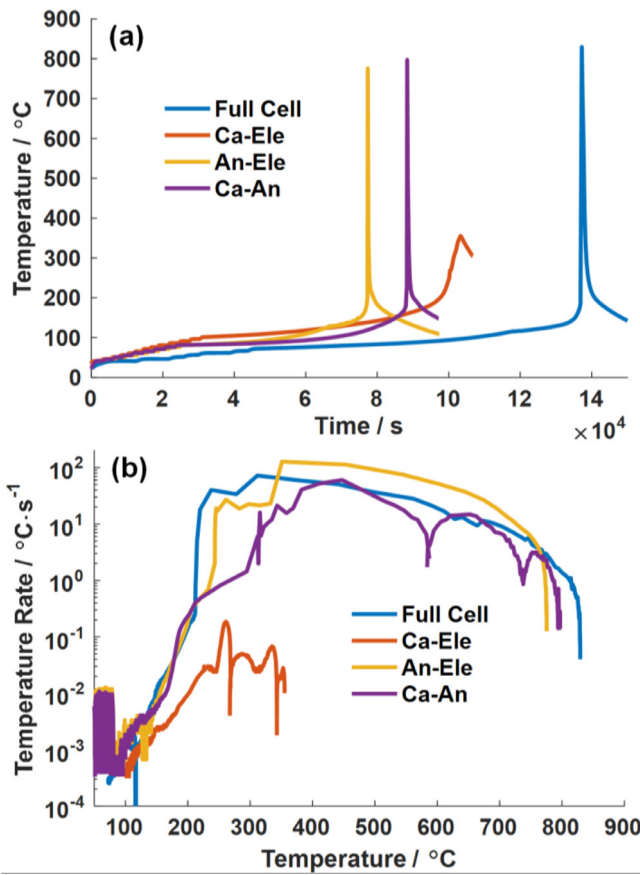


**Fig. 8.** TR test results of partial cells. (a) temperature profiles; (b) temperature rate profiles. The An-Ele and Ca-An partial cells went into TR, indicating that the exothermic reactions in An-Ele and Ca-An thermodynamic systems were the dominant heat sources of TR. The An-Ele partial cell had a  $T_2$  close to that of the full cell, and was responsible for triggering battery TR.

that the exothermic reactions in An-Ele and Ca-An thermodynamic systems were the dominant heat sources of TR. In contrast, the reactions between cathode and electrolyte had small contribution to TR, due to the vaporization of the solvents (the boiling temperatures of DMC, EMC and EC are 91 °C, 110 °C and 248 °C, respectively) before the release of oxygen from the  $\text{Li}(\text{NiCoMn})_{1/3}\text{O}_2$  cathode at around 250 °C [21]. Moreover, the An-Ele partial cell had a  $T_2$  of 243.5°C, close to that of full cell, while the Ca-An partial cell did not go into TR until 314.7°C. Therefore, we can confirm that the reactions between anode

and electrolyte were responsible for triggering TR inside the battery. The redox reactions between cathode and anode started later and contributed to the total heat generation. That is different from the conventional views that redox reaction induced by the oxygen released from the layered cathode or ISC is the trigger of battery TR [25,34,63], and reminds us of the contribution of exothermic reactions on the anode when investigating the initiation mechanism of battery TR.

Based on the above analysis, we can summarize the battery TR mechanism and divide the TR process into four stages accordingly, as shown in Fig. 9.

**Stage I:** The battery starts self-heating due to exothermic reactions on the anode, including decomposition of SEI film and the reaction between lithiated graphite and electrolyte. Electrolyte decomposition and evaporation of low boiling-point solvents also proceed inside the battery, resulting in increase of battery impedance. The separator shows no shrinkage as the temperature is lower than the melting point of PE.

**Stage II:** ISC happens on the battery as the separator shrinks severely due to PE melting, leading to an instant drop in battery voltage. However, as the battery impedance has increased about 1000 times, a little amount of joule heat is released through ISC. Thus, there is no obvious increase in battery temperature rate.

**Stage III:** The reactions between lithiated graphite and electrolyte proceed as battery temperature goes higher. The An-Ele reactions release a large amount of heat and then triggers battery TR.

**Stage IV:** Redox reactions between Ca-An begin once the cathode starts releasing oxygen at elevated temperature, leading to further heat generation and bringing the battery temperature to  $T_3$  rapidly.

### 3.5. Discussion on the relationship between internal short circuit and thermal runaway

According to the above analysis, the amount of joule heat released from ISC is limited by the significantly-increased battery resistance. In this section, the relationship between ISC and TR is further discussed through simulation by varying battery resistance, as shown in Fig. 10. A 3D electrochemical-thermal coupled ISC model established in our previous paper [47] is implemented to qualitatively investigate the ISC behaviors of lithium-ion battery. More details of the model are presented in the *Supplementary Material*. The battery voltage is simulated by a pseudo-two-dimensional (P2D) model, while heat generation mainly originates from joule heat by ISC [47]. In the 3D model, ISC occurs on the edge of the mid-plane with an area of  $5 \times 5 \text{ mm}^2$  with an equivalent ISC resistance  $R_{\text{ISC}}$  of  $15\text{m}\Omega$ , as illustrated in Fig. 10(d). The value of  $R_{\text{ISC}}$  is estimated according to the battery voltage drop from around 4 V to 0.04 V when ISC occurred in Fig. 7. It should be noted that heat generation from exothermic reactions between cathode, anode, and electrolyte is neglected in this simulation, as we mainly focus on the heat generation from ISC. The battery resistance is adjusted by regulating the electrical conductivities in solid and electrolyte phase, as presented in Fig. 10.  $R_0 = 1.5\text{m}\Omega$  is the initial value of battery resistance.

Battery voltage shows an instant drop when ISC happens, and the falling speed increases with the rise of battery resistance, as shown in Fig. 10(a). Meanwhile, the whole jelly roll exhibits a slight temperature rise, which decreases as battery resistance increases, as in Fig. 10(b). That indicates that only a small amount of joule heat is generated from ISC, which is not enough to bring the whole battery to TR. However, significant local temperature rise can be observed in the ISC area, as showed in Fig. 10(c). Fig. 10(d)~(i) present the temperature distribution in the mid-plane when ISC occurs. As shown in Fig. 10(d) and (e), the battery with small resistance ( $R = R_0, 5R_0$ ) shows a maximum temperature rise larger than 100°C, which is large enough to trigger TR in the ISC area (suppose ISC occurs at a temperature higher than 100°C during TR process). A large amount of heat generation from local TR

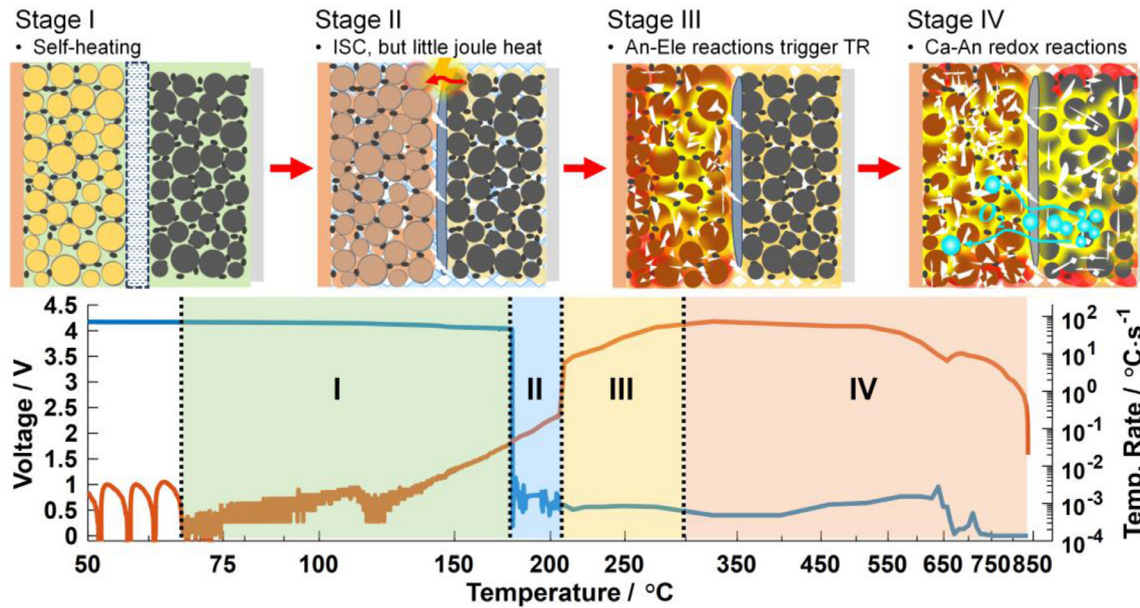


**Fig. 9.** The four-stage TR mechanism of lithium-ion battery. (Stage I) The battery starts self-heating due to the decomposition of SEI film; (Stage II) ISC occurs when separator shrinks severely, but generates little amount of joule heat; (Stage III) Heat generation from An-Ele reactions increases at elevated temperature, triggering TR; (Stage IV) Redox reactions between Ca-An begin, bringing the battery temperature to  $T_3$  rapidly.

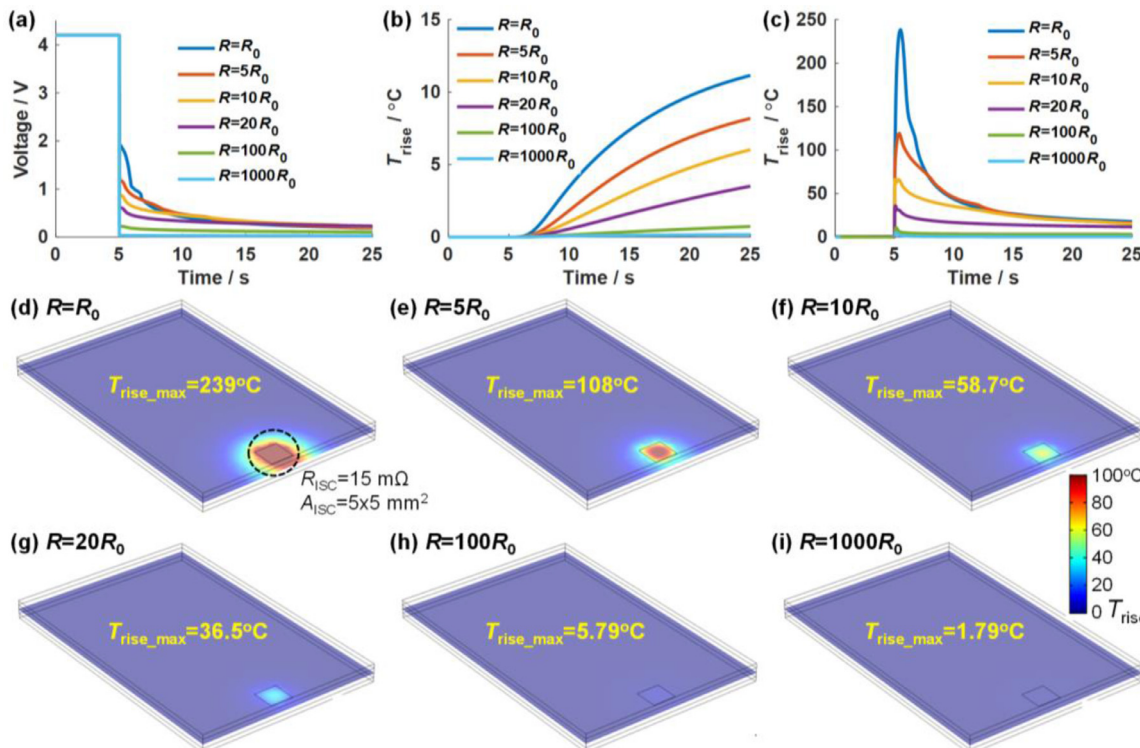


**Fig. 10.** Simulation results of ISC behaviors of the battery with different resistance. (a) change of battery voltage during ISC; (b) battery temperature rise measured at the center of the jelly roll; (c) local temperature rise measured at the center of the ISC area. Significant local temperature rise can be observed; (d)–(i) temperature distribution in the mid-plane 0.5 s after ISC occurs. For the batteries with a small resistance ( $R = R_0, 5R_0$ ), the maximum temperature rise is larger than 100°C and is enough to trigger local TR. For the batteries with a resistance of 10 or 20 times its initial value, and temperature rise is limited in the ISC area, as shown in Fig. 10(f) and (g). As the battery resistance increases to a higher value

can spread from the ISC area to the whole jelly roll rapidly due to the excellent thermal conductivity of Al and Cu collectors, leading to subsequent TR of the whole battery [48]. The battery shows decreased local temperature rise when the battery resistance increased to 10 or 20 times its initial value, and temperature rise is limited in the ISC area, as shown in Fig. 10(f) and (g). As the battery resistance increases to a higher value

( $100R_0, 1000R_0$ ), the maximum local temperature rise decreases to less than 10°C, as in Fig. 10(h) and (i). ISC has no obvious contribution to battery TR in those two cases, similar with the TR test results of the 24Ah lithium-ion battery. According to the above simulation results, we can conclude that the contribution of ISC to battery TR is significantly influenced by battery resistance when ISC occurs. A large battery

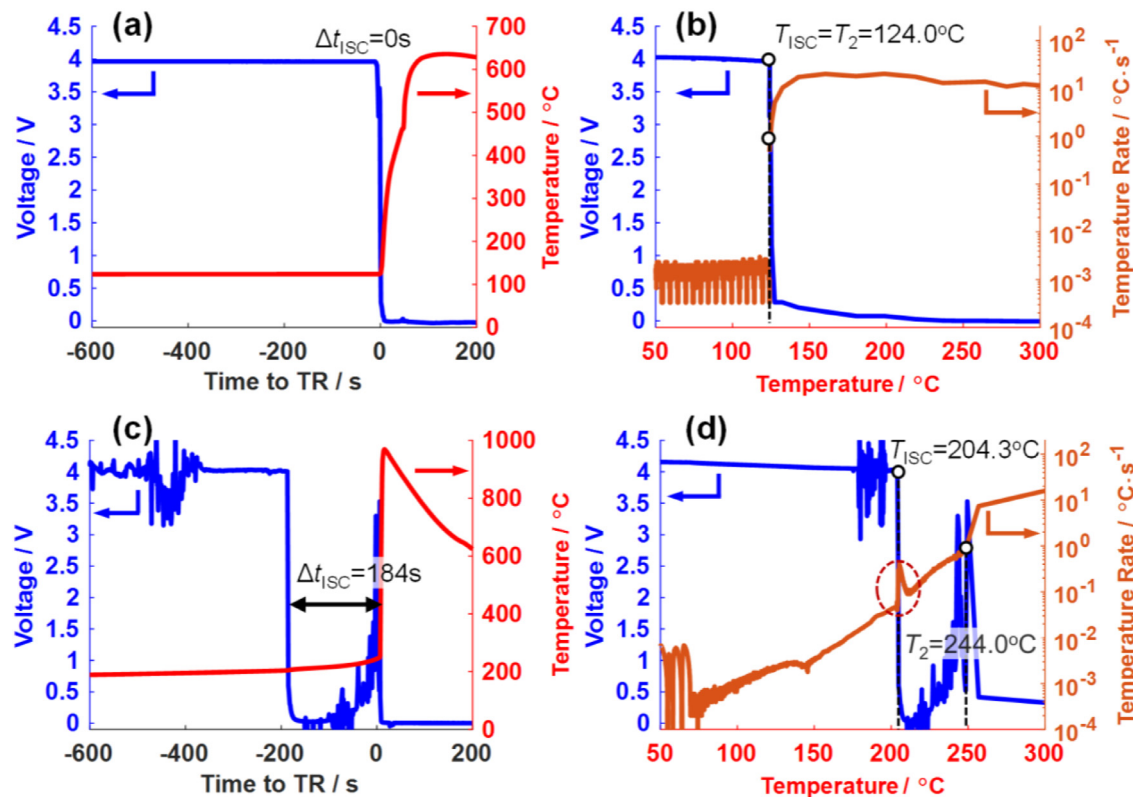


**Fig. 11.** Thermal runaway test results to validate the modeling analysis on the influence of ISC on battery TR. (a) and (b) TR behavior of a lithium-ion battery with a bare PE separator. ISC occurred at  $124.0^\circ\text{C}$  when shrinkage of PE started, generating a large amount of heat and leading to TR directly; (c) and (d) TR behavior of a lithium-ion battery with high boiling point electrolyte. ISC occurred at  $204.3^\circ\text{C}$  and led to a small peak in the temperature rate profile.

resistance can help to reduce the joule heat generation from ISC and improve battery tolerance to ISC.

Fig. 11 presents some TR test results of lithium-ion battery that can validate the modeling analysis on the influence of ISC. Fig. 11(a) and (b) are the TR test results of a 21Ah lithium-ion battery with  $\text{LiNi}_x\text{Co}_y\text{Mn}_z\text{O}_2$  cathode and graphite anode. The 21Ah lithium-ion battery had a bare PE separator with poor thermal stability [36]. As shown in Fig. 11(b), ISC occurred at  $124.0^\circ\text{C}$  when shrinkage of PE started. The battery had a low resistance at  $124.0^\circ\text{C}$ , as the majority of the electrolyte remained inside. Therefore, ISC generated a large amount of joule heat, leading to local TR in the ISC area and further TR propagation among the whole battery, as shown in Fig. 11(a) and (b), similar with the simulation cases in Fig. 10(d) and (e). Fig. 11(c) and (d) show the TR test results of a 3.3Ah lithium-ion battery with high boiling point electrolyte. The 3.3Ah lithium-ion battery had  $\text{LiNi}_x\text{Co}_y\text{Mn}_z\text{O}_2$  cathode, graphite anode and a PE-based separator with ceramic coating, and the electrolyte was composed of 1.0 M  $\text{LiPF}_6$  in ethylene EC / polycarbonate (PC) / diethyl carbonate (DEC) (1:1:1 in volume). Compared to the electrolyte (1.0 M  $\text{LiPF}_6$  in EC/EMC/DMC) of the 24 Ah lithium-ion battery, the electrolyte of the 3.3Ah lithium-ion battery had more high boiling point solvents (EC and PC), as the boiling point of EC, EMC, DMC, PC, DEC are  $248^\circ\text{C}$ ,  $110^\circ\text{C}$ ,  $91^\circ\text{C}$ ,  $242^\circ\text{C}$ ,  $126^\circ\text{C}$ , respectively [64]. During the ARC test of the 3.3Ah lithium-ion battery, ISC occurred at  $204.3^\circ\text{C}$  and did not cause TR directly. However, as in Fig. 11(d), ISC did lead to a small peak in the temperature rate profile, different from the little heat generation from ISC in Fig. 3, mainly due to the difference in electrolyte inside the two cells. The 3.3Ah battery has more remaining electrolyte and thus a smaller resistance than the 24Ah battery when ISC occurred between  $170\text{--}200^\circ\text{C}$ , resulting in a relatively larger amount of joule heat from ISC. The test results presented in Fig. 11(a)–(d) are consistent with the simulation results in Fig. 10, further convincing us that the amount of

joule heat from ISC and its contribution to TR significantly depend on battery resistance during the occurrence of ISC.

#### 4. Conclusion

This paper presents a comprehensive investigation of the relationship between ISC and TR of lithium-ion battery under thermal abuse condition. The contribution of ISC to TR and the root cause of TR are characterized through a series of TR tests and materials characterization. Possible factors that affect heat generation from ISC are also discussed based on a 3D electrochemical-thermal coupled ISC model.

During ARC test on a 24Ah commercial pouch lithium-ion battery, ISC was observed to happen 300 s before TR but showed no apparent contribution to battery temperature rate profile. Evidence of ISC can be found at the edge of the electrodes after freezing the battery at  $T_{ISC}$ , due to severe thermal shrinkage of the separator. However, the electrochemical test results on cathode and anode materials showed that most of the energy was still stored inside the battery, demonstrating that only a small amount of energy was released through ISC. Moreover, the battery experienced a sharp increase (around 1000 times) of resistance before ISC, due to depletion of electrolyte, porosity reduction of electrodes, and shutdown of separator. The increased battery resistance limits the short circuit current to a small value. Thus, ISC leads to little joule heat generation and is not responsible for battery TR.

Partial cells with different mixtures of cell components were tested to characterize the root cause of TR. The An-Ele and Ca-An partial cells both went into TR, indicating that the anode-electrolyte and cathode-anode thermodynamic systems are the dominant heat sources during TR process. Moreover, the exothermic reactions between anode and electrolyte are identified as the trigger of battery TR, as the An-Ele partial cell exhibits a lower  $T_2$  than the Ca-An partial cell. The redox reactions

between cathode and anode start at a higher temperature and contribute to the total heat generation. The result is different from the conventional views that oxygen released from cathode or ISC is the critical reason for battery TR, and provide a new finding of the trigger mechanism of battery TR.

Finally, a discussion on the effect of ISC on TR for the battery with different designs is presented based on a 3D electrochemical-thermal coupled ISC model. Two more TR test results of different lithium-ion batteries were performed to validate the simulation results. The contribution of ISC to battery TR is significantly influenced by battery resistance when ISC occurs. A large battery resistance can help to reduce the joule heat generation from ISC and improve battery tolerance to ISC.

## Declaration of Competing Interest

The authors declare that they have no known competing financial interests or personal relationships that could have appeared to influence the work reported in this paper.

## CRediT authorship contribution statement

**Dongsheng Ren:** Conceptualization, Methodology, Investigation, Data curation, Writing - original draft. **Xuning Feng:** Conceptualization, Methodology, Formal analysis. **Lishuo Liu:** Methodology, Software, Formal analysis. **Hungjen Hsu:** Investigation, Data curation. **Languang Lu:** Writing - review & editing. **Li Wang:** Writing - review & editing. **Xiangming He:** Writing - review & editing, Resources. **Minggao Ouyang:** Supervision, Conceptualization, Resources.

## Acknowledgement

The work is supported by the Ministry of Science and Technology of China (No. 2019YFE0100200 and 2019YFA0705703), the National Natural Science Foundation of China (No. 51706117, and 51807108), and the Tsinghua University Initiative Scientific Research Program (No. 2019Z02UTY06). The Authors would also like to acknowledge the financial support of Tsinghua University-Zhangjiagang Joint Institute for Hydrogen Energy and Lithium-Ion Battery Technology (JHLT).

## Supplementary materials

Supplementary material associated with this article can be found, in the online version, at doi:[10.1016/j.ensm.2020.10.020](https://doi.org/10.1016/j.ensm.2020.10.020).

## References

- [1] X.Y. Shan, F. Li, D.W. Wang, H.M. Cheng, The smart era of electrochemical energy storage devices, *Energy Storage Mater* 3 (2016) 66–68, doi:[10.1016/j.ensm.2016.01.005](https://doi.org/10.1016/j.ensm.2016.01.005).
- [2] J. Dixon, K. Bell, Electric vehicles: battery capacity, charger power, access to charging and the impacts on distribution networks, *eTransportation*, 4, 2020, doi:[10.1016/j.etrans.2020.100059](https://doi.org/10.1016/j.etrans.2020.100059).
- [3] J.B. Goodenough, Energy storage materials: a perspective, *Energy Storage Mater* 1 (2015) 158–161, doi:[10.1016/j.ensm.2015.07.001](https://doi.org/10.1016/j.ensm.2015.07.001).
- [4] S. Tanaka, K. Nagumo, M. Yamamoto, H. Chiba, K. Yoshida, R. Okano, Fuel cell system for Honda CLARITY fuel cell, *eTransportation*, 3, 2020, doi:[10.1016/j.etrans.2020.100046](https://doi.org/10.1016/j.etrans.2020.100046).
- [5] X. Feng, Y. Merla, C. Weng, M. Ouyang, X. He, B.Y. Liaw, et al., A reliable approach of differentiating discrete sampled-data for battery diagnosis, *eTransportation* 3 (2020) 100051, doi:[10.1016/j.etrans.2020.100051](https://doi.org/10.1016/j.etrans.2020.100051).
- [6] X. Feng, M. Ouyang, X. Liu, L. Lu, Y. Xia, X. He, Thermal runaway mechanism of lithium ion battery for electric vehicles: a review, *Energy Storage Mater* 10 (2018) 246–267, doi:[10.1016/j.ensm.2017.05.013](https://doi.org/10.1016/j.ensm.2017.05.013).
- [7] L. Jiang, X.-B. Cheng, H.-J. Peng, J.-Q. Huang, Q. Zhang, Carbon materials for traffic power battery, *eTransportation*, 2, 2019, doi:[10.1016/j.etrans.2019.100033](https://doi.org/10.1016/j.etrans.2019.100033).
- [8] X. Han, L. Lu, Y. Zheng, X. Feng, Z. Li, J. Li, et al., A review on the key issues of the lithium ion battery degradation among the whole life cycle, *eTransportation*, 1, 2019, doi:[10.1016/j.etrans.2019.100005](https://doi.org/10.1016/j.etrans.2019.100005).
- [9] Y. Lu, X. Rong, Y.S. Hu, L. Chen, H. Li, Research and development of advanced battery materials in China, *Energy Storage Mater* 23 (2019) 144–153, doi:[10.1016/j.ensm.2019.05.019](https://doi.org/10.1016/j.ensm.2019.05.019).
- [10] X. Feng, D. Ren, X. He, M. Ouyang, Mitigating thermal runaway of lithium-ion batteries, in: *Joule*, 4, 2020, pp. 743–770, doi:[10.1016/j.joule.2020.02.010](https://doi.org/10.1016/j.joule.2020.02.010).
- [11] P. Lyu, X. Liu, J. Qu, J. Zhao, Y. Huo, Z. Qu, et al., Recent advances of thermal safety of lithium ion battery for energy storage, *Energy Storage Mater* (2020), doi:[10.1016/j.ensm.2020.06.042](https://doi.org/10.1016/j.ensm.2020.06.042).
- [12] Q. Wang, P. Ping, X. Zhao, G. Chu, J. Sun, C. Chen, Thermal runaway caused fire and explosion of lithium ion battery, *J. Power Sources*. 208 (2012) 210–224, doi:[10.1016/j.jpowsour.2012.02.038](https://doi.org/10.1016/j.jpowsour.2012.02.038).
- [13] B. Liu, Y. Jia, C. Yuan, L. Wang, X. Gao, S. Yin, et al., Safety issues and mechanisms of lithium-ion battery cell upon mechanical abusive loading: a review, *Energy Storage Mater* 24 (2020) 85–112, doi:[10.1016/j.ensm.2019.06.036](https://doi.org/10.1016/j.ensm.2019.06.036).
- [14] X. Huang, J. Xue, M. Xiao, S. Wang, Y. Li, S. Zhang, et al., Comprehensive evaluation of safety performance and failure mechanism analysis for lithium sulfur pouch cells, *Energy Storage Mater* 30 (2020) 87–97, doi:[10.1016/j.ensm.2020.04.035](https://doi.org/10.1016/j.ensm.2020.04.035).
- [15] A. Mallarapu, J. Kim, K. Carney, P. DuBois, S. Santhanagopalan, Modeling extreme deformations in lithium ion batteries, *eTransportation*, 4, 2020, doi:[10.1016/j.etrans.2020.100065](https://doi.org/10.1016/j.etrans.2020.100065).
- [16] W. Mei, L. Zhang, J. Sun, Q. Wang, Experimental and numerical methods to investigate the overcharge caused lithium plating for lithium ion battery, *Energy Storage Mater*, 2020, doi:[10.1016/j.ensm.2020.06.021](https://doi.org/10.1016/j.ensm.2020.06.021).
- [17] D. Ren, X. Feng, L. Lu, X. He, M. Ouyang, Overcharge behaviors and failure mechanism of lithium-ion batteries under different test conditions, *Appl. Energy*. 250 (2019) 323–332, doi:[10.1016/j.apenergy.2019.05.015](https://doi.org/10.1016/j.apenergy.2019.05.015).
- [18] Q. Wang, L. Jiang, Y. Yu, J. Sun, Progress of enhancing the safety of lithium ion battery from the electrolyte aspect, *Nano Energy* 55 (2018) 93–114, doi:[10.1016/j.nanoen.2018.10.035](https://doi.org/10.1016/j.nanoen.2018.10.035).
- [19] G. Xu, L. Huang, C. Lu, X. Zhou, G. Cui, Revealing the multilevel thermal safety of lithium batteries, *Energy Storage Mater* 31 (2020) 72–86, doi:[10.1016/j.ensm.2020.06.004](https://doi.org/10.1016/j.ensm.2020.06.004).
- [20] W. Li, J. Zhu, Y. Xia, M.B. Gorji, T. Wierzbicki, Data-driven safety envelope of lithium-ion batteries for electric vehicles, *Joule* (2019) 1–13, doi:[10.1016/j.joule.2019.07.026](https://doi.org/10.1016/j.joule.2019.07.026).
- [21] D. Ren, X. Liu, X. Feng, L. Lu, M. Ouyang, J. Li, et al., Model-based thermal runaway prediction of lithium-ion batteries from kinetics analysis of cell components, *Appl. Energy*. 228 (2018) 633–644, doi:[10.1016/j.apenergy.2018.06.126](https://doi.org/10.1016/j.apenergy.2018.06.126).
- [22] E.P. Roth, D.H. Doughty, Thermal abuse performance of high-power 18650 Li-ion cells, *J. Power Sources*. 128 (2004) 308–318, doi:[10.1016/j.jpowsour.2003.09.068](https://doi.org/10.1016/j.jpowsour.2003.09.068).
- [23] D.H. Doughty, E.P. Roth, C.C. Crafts, G. Nagasubramanian, G. Henriksen, K. Amine, Effects of additives on thermal stability of Li ion cells, *J. Power Sources*. 146 (2005) 116–120, doi:[10.1016/j.jpowsour.2005.03.170](https://doi.org/10.1016/j.jpowsour.2005.03.170).
- [24] X. Feng, M. Fang, X. He, M. Ouyang, L. Lu, H. Wang, et al., Thermal runaway features of large format prismatic lithium ion battery using extended volume accelerating rate calorimetry, *J. Power Sources*. 255 (2014) 294–301, doi:[10.1016/j.jpowsour.2014.01.005](https://doi.org/10.1016/j.jpowsour.2014.01.005).
- [25] X. Feng, S. Zheng, D. Ren, X. He, L. Wang, H. Cui, et al., Investigating the thermal runaway mechanisms of lithium-ion batteries based on thermal analysis database, *Appl. Energy*. 246 (2019) 53–64, doi:[10.1016/j.apenergy.2019.04.009](https://doi.org/10.1016/j.apenergy.2019.04.009).
- [26] X. Feng, S. Zheng, X. He, L. Wang, Y. Wang, D. Ren, et al., Time sequence map for interpreting the thermal runaway mechanism of lithium-ion batteries with LiNi<sub>x</sub>CoyMn<sub>2-x</sub>O<sub>2</sub> cathode, *Front. Energy Res.* 6 (2018) 1–16, doi:[10.3389/fenrg.2018.00126](https://doi.org/10.3389/fenrg.2018.00126).
- [27] M.N. Richard, J.R. Dahn, Accelerating rate calorimetry study on the thermal stability of lithium intercalated graphite in electrolyte. I. Experimental, *J. Electrochem. Soc.* 146 (1999) 2068–2077, doi:[10.1149/1.1391894](https://doi.org/10.1149/1.1391894).
- [28] Z. Chen, Y. Qin, Y. Ren, W. Lu, C. Orendorff, E.P. Roth, et al., Multi-scale study of thermal stability of lithiated graphite, *Energy Environ. Sci.* 4 (2011) 4023–4030, doi:[10.1039/clee01786a](https://doi.org/10.1039/clee01786a).
- [29] Q. Wang, J. Sun, X. Yao, C. Chen, Thermal behavior of lithiated graphite with electrolyte in lithium-ion batteries, *J. Electrochem. Soc.* 153 (2006) A329–A333, doi:[10.1149/1.2139955](https://doi.org/10.1149/1.2139955).
- [30] S. Bak, E. Hu, Y. Zhou, X. Yu, S.D. Senanayake, S. Cho, et al., Structural changes and thermal stability of charged LiNi<sub>x</sub>Mn<sub>y</sub>Co<sub>z</sub>O<sub>2</sub> cathode materials studied by combined in situ time-resolved XRD and mass spectroscopy, in: *ACS Appl. Mater. Interfaces*, 6, 2014, pp. 22594–22601, doi:[10.1021/am506712c](https://doi.org/10.1021/am506712c).
- [31] A. Manthiram, B. Song, W. Li, A perspective on nickel-rich layered oxide cathodes for lithium-ion batteries, *Energy Storage Mater* 6 (2017) 125–139, doi:[10.1016/j.ensm.2016.10.007](https://doi.org/10.1016/j.ensm.2016.10.007).
- [32] S.S. Zhang, Problems and their origins of Ni-rich layered oxide cathode materials, *Energy Storage Mater* 24 (2020) 247–254, doi:[10.1016/j.ensm.2019.08.013](https://doi.org/10.1016/j.ensm.2019.08.013).
- [33] Q. Huang, L. Ma, A. Liu, X. Ma, J. Li, J. Wang, et al., The reactivity of charged positive Li<sub>1-n</sub>[Ni<sub>x</sub>Mn<sub>y</sub>Co<sub>z</sub>]O<sub>2</sub> electrodes with electrolyte at elevated temperatures using accelerating rate calorimetry, *J. Power Sources*. 390 (2018) 78–86, doi:[10.1016/j.jpowsour.2018.04.036](https://doi.org/10.1016/j.jpowsour.2018.04.036).
- [34] X. Liu, D. Ren, H. Hsu, X. Feng, G.L. Xu, M. Zhuang, et al., Thermal runaway of lithium-ion batteries without internal short circuit, *Joule* (2018) 1–18, doi:[10.1016/j.joule.2018.06.015](https://doi.org/10.1016/j.joule.2018.06.015).
- [35] T. Inoue, K. Mukai, Roles of positive or negative electrodes in the thermal runaway of lithium-ion batteries: accelerating rate calorimetry analyses with an all-inclusive microcell, *Electrochim. Commun.* 77 (2017) 28–31, doi:[10.1016/j.elecom.2017.02.008](https://doi.org/10.1016/j.elecom.2017.02.008).
- [36] C.M. Costa, Y.H. Lee, J.H. Kim, S.Y. Lee, S. Lanceros-Méndez, Recent advances on separator membranes for lithium-ion battery applications: from porous membranes to solid electrolytes, *Energy Storage Mater* 22 (2019) 346–375, doi:[10.1016/j.ensm.2019.07.024](https://doi.org/10.1016/j.ensm.2019.07.024).
- [37] E.P. Roth, D.H. Doughty, D.L. Pile, Effects of separator breakdown on abuse response of 18650 Li-ion cells, *J. Power Sources*. 174 (2007) 579–583, doi:[10.1016/j.jpowsour.2007.06.163](https://doi.org/10.1016/j.jpowsour.2007.06.163).

- [38] H. Maleki, G. Deng, A. Anani, J. Howard, Thermal stability studies of Li-ion cells and components, *J. Electrochem. Soc.* 146 (1999) 3224–3229, doi:[10.1149/1.1392458](https://doi.org/10.1149/1.1392458).
- [39] Y. Li, X. Feng, D. Ren, M. Ouyang, L. Lu, X. Han, Thermal runaway triggered by plated lithium on the anode after fast charging, in: *ACS Appl. Mater. Interfaces*, 11, 2019, pp. 46839–46850, doi:[10.1021/acsami.9b16589](https://doi.org/10.1021/acsami.9b16589).
- [40] D. Ren, H. Hsu, R. Li, X. Feng, D. Guo, X. Han, et al., A comparative investigation of aging effects on thermal runaway behavior of lithium-ion batteries, *eTransportation*, 2, 2019, doi:[10.1016/j.etrans.2019.100034](https://doi.org/10.1016/j.etrans.2019.100034).
- [41] A. Tomaszecka, Z. Chu, X. Feng, S. O’Kane, X. Liu, J. Chen, et al., Lithium-ion battery fast charging: a review, *eTransportation* 1 (2019) 100011, doi:[10.1016/j.etrans.2019.100011](https://doi.org/10.1016/j.etrans.2019.100011).
- [42] P.T. Coman, E.C. Darcy, C.T. Veje, R.E. White, Modelling Li-ion cell thermal runaway triggered by an internal short circuit device using an efficiency factor and arrhenius formulations, *J. Electrochem. Soc.* 164 (2017) A587–A593, doi:[10.1149/2.0341704jes](https://doi.org/10.1149/2.0341704jes).
- [43] D.P. Finegan, E. Darcy, M. Keyser, B. Tjaden, T.M.M. Heenan, R. Jervis, et al., Characterising thermal runaway within lithium-ion cells by inducing and monitoring internal short circuits, *Energy Environ. Sci.* 10 (2017) 1377–1388, doi:[10.1039/c7ee00385d](https://doi.org/10.1039/c7ee00385d).
- [44] D.P. Finegan, B. Tjaden, T.M.M. Heenan, R. Jervis, M. Di Michiel, A. Rack, et al., Tracking internal temperature and structural dynamics during nail penetration of lithium-ion cells, *J. Electrochem. Soc.* 164 (2017) A3285–A3291, doi:[10.1149/2.1501713jes](https://doi.org/10.1149/2.1501713jes).
- [45] M. Naguib, S. Allu, S. Simunovic, J. Li, H. Wang, N.J. Dudney, Limiting internal short-circuit damage by electrode partition for impact-tolerant Li-ion batteries, *Joule* 2 (2018) 155–167, doi:[10.1016/j.joule.2017.11.003](https://doi.org/10.1016/j.joule.2017.11.003).
- [46] R. Guo, L. Lu, M. Ouyang, X. Feng, Mechanism of the entire overdischarge process and overdischarge-induced internal short circuit in lithium-ion batteries, *Sci. Rep.* 6 (2016) 30248, doi:[10.1038/srep30248](https://doi.org/10.1038/srep30248).
- [47] L. Liu, X. Feng, M. Zhang, L. Lu, X. Han, X. He, et al., Comparative study on substitute triggering approaches for internal short circuit in lithium-ion batteries, *Appl. Energy*. 259 (2020) 114143, doi:[10.1016/j.apenergy.2019.114143](https://doi.org/10.1016/j.apenergy.2019.114143).
- [48] S. Santhanagopalan, P. Ramadas, J. Zhang, Analysis of internal short-circuit in a lithium ion cell, *J. Power Sources*. 194 (2009) 550–557, doi:[10.1016/j.jpowsour.2009.05.002](https://doi.org/10.1016/j.jpowsour.2009.05.002).
- [49] E. Wang, H.-P. Wu, C.-H. Chiu, P.-H. Chou, The effect of battery separator properties on thermal ramp, overcharge and short circuiting of rechargeable Li-ion batteries, *J. Electrochem. Soc.* 166 (2019) A125–A131, doi:[10.1149/2.0381902jes](https://doi.org/10.1149/2.0381902jes).
- [50] J. Zhang, L. Su, Z. Li, Y. Sun, N. Wu, The evolution of lithium-ion cell thermal safety with aging examined in a battery testing calorimeter, *Batteries* 2 (2016) 12, doi:[10.3390/batteries2020012](https://doi.org/10.3390/batteries2020012).
- [51] S. Zheng, L. Wang, X. Feng, X. He, Probing the heat sources during thermal runaway process by thermal analysis of different battery chemistries, *J. Power Sources*. 378 (2018) 527–536, doi:[10.1016/j.jpowsour.2017.12.050](https://doi.org/10.1016/j.jpowsour.2017.12.050).
- [52] M. Zhang, J. Du, L. Liu, A. Stefanopoulou, J. Siegel, L. Lu, et al., Internal short circuit trigger method for lithium-ion battery based on shape memory alloy, *J. Electrochem. Soc.* 164 (2017) A3038–A3044, doi:[10.1149/2.0731713jes](https://doi.org/10.1149/2.0731713jes).
- [53] P.T. Coman, S. Rayman, R.E. White, A lumped model of venting during thermal runaway in a cylindrical lithium cobalt oxide lithium-ion cell, *J. Power Sources*. 307 (2016) 56–62, doi:[10.1016/j.jpowsour.2015.12.088](https://doi.org/10.1016/j.jpowsour.2015.12.088).
- [54] R. Spotnitz, J. Franklin, Abuse behavior of high-power, lithium-ion cells, *J. Power Sources*. 113 (2003) 81–100, doi:[10.1016/S0378-7753\(02\)00488-3](https://doi.org/10.1016/S0378-7753(02)00488-3).
- [55] K. Son, S.M. Hwang, S.G. Woo, J.K. Koo, M. Paik, E.H. Song, et al., Comparative study of thermal runaway and cell failure of lab-scale Li-ion batteries using accelerating rate calorimetry, *J. Ind. Eng. Chem.* 83 (2020) 247–251, doi:[10.1016/j.jiec.2019.11.034](https://doi.org/10.1016/j.jiec.2019.11.034).
- [56] Y.-S. Duh, X. Liu, X. Jiang, C.-S. Kao, L. Gong, R. Shi, Thermal kinetics on exothermic reactions of a commercial LiCoO<sub>2</sub> 18650 lithium-ion battery and its components used in electric vehicles: a review, *J. Energy Storage*. 30 (2020) 101422, doi:[10.1016/j.est.2020.101422](https://doi.org/10.1016/j.est.2020.101422).
- [57] K.E. Thomas-Alyea, C. Jung, R.B. Smith, M.Z. Bazant, Situ Observation and Mathematical Modeling of Lithium Distribution within Graphite, *J. Electrochem. Soc.* 164 (2017) E3063–E3072, doi:[10.1149/2.0061711jes](https://doi.org/10.1149/2.0061711jes).
- [58] X. Feng, J. Sun, M. Ouyang, X. He, L. Lu, X. Han, et al., Characterization of large format lithium ion battery exposed to extremely high temperature, *J. Power Sources*. 272 (2014) 457–467, doi:[10.1016/j.jpowsour.2014.08.094](https://doi.org/10.1016/j.jpowsour.2014.08.094).
- [59] C. Shi, J. Dai, C. Li, X. Shen, L. Peng, P. Zhang, et al., A modified ceramic-coating separator with high-temperature stability for lithium-ion battery, *Polymers (Basel)* 9 (2017) 10–14, doi:[10.3390/polym9050159](https://doi.org/10.3390/polym9050159).
- [60] H. Yang, G.V. Zhuang, P.N. Ross, Thermal stability of LiPF<sub>6</sub> salt and Li-ion battery electrolytes containing LiPF<sub>6</sub>, *J. Power Sources*. 161 (2006) 573–579, doi:[10.1016/j.jpowsour.2006.03.058](https://doi.org/10.1016/j.jpowsour.2006.03.058).
- [61] I. Bloom, J. Bareño, N. Dietz Rago, F. Dogan, D.G. Graczyk, Y. Tsai, et al., Effect of overcharge on lithium-ion cells containing Li(Ni<sub>0.5</sub>Mn<sub>0.3</sub>Co<sub>0.2</sub>)O<sub>2</sub> cathodes: nMP-soluble binder. II - Chemical changes in the anode, *J. Power Sources*. 385 (2018) 156–164, doi:[10.1016/j.jpowsour.2017.12.015](https://doi.org/10.1016/j.jpowsour.2017.12.015).
- [62] P. Arora, Z. Zhang, Battery separators, *Chem. Rev.* 104 (2004) 4419–4462, doi:[10.1021/cr020738u](https://doi.org/10.1021/cr020738u).
- [63] Q. Wang, B. Mao, S.I. Stoliarov, J. Sun, A review of lithium ion battery failure mechanisms and fire prevention strategies, *Prog. Energy Combust. Sci.* 73 (2019) 95–131, doi:[10.1016/j.pecs.2019.03.002](https://doi.org/10.1016/j.pecs.2019.03.002).
- [64] G.G. Eshetu, S. Gruegeon, S. Laruelle, S. Boyanov, A. Lecocq, J.-P. Bertrand, et al., In-depth safety-focused analysis of solvents used in electrolytes for large scale lithium ion batteries, *Phys. Chem. Chem. Phys.* 15 (2013) 9145–9155, doi:[10.1039/c3cp51315g](https://doi.org/10.1039/c3cp51315g).